Journal of Cleaner Production 421 (2023) 138448

Contents lists available at ScienceDirect

Journal of Cleaner Production

journal homepage: www.elsevier.com/locate/jclepro

# Treatment of textile dye via economic fungi/MCM-41 bio-based adsorbent: Application of neural network approach

Veli Şimşek [a,b], Rahmiye Zerrin Yarbay [a,c], Vedat Marttin [d], Ülküye Dudu Gül [e,*]

[a] Department of Chemical Engineering, Faculty of Engineering, Bilecik Seyh Edebali University, 11230, Bilecik, Turkey
[b] Biotechnology Application and Research Centre, Bilecik Seyh Edebali University, 11230, Bilecik, Turkey
[c] Energy Technologies Application and Research Centre, Bilecik Seyh Edebali University, 11210, Bilecik, Turkey
[d] Department of Computer Engineering, Faculty of Engineering, Bilecik Seyh Edebali University, 11230, Bilecik, Turkey
[e] Department of Bioengineering, Faculty of Engineering, Bilecik Seyh Edebali University, 11230, Bilecik, Turkey

ARTICLE INFO

Handling Editor: Hua Cai

*Keywords:*
Bioadsorbent
MCM-41
Artificial neural network (ANN) modeling
Decolorization
*Suillus collinitus*
Reactive red 120

ABSTRACT

There has been an increased interest in developing environmentally friendly and cost-effective technologies for treating water contaminated with dyes found in textile industry wastewater. The adsorption mechanism allows the use of cheap adsorbents. In particular, using bioadsorbents developed with biocompatible materials is an environmentally friendly approach. This study aims to determine the textile dye Reactive Red 120 (RR120) removal capacity of a novel bio-based adsorbent developed by combining an effective catalyst and naturally available fungal wastes at the batch scale level. For this purpose, morphological and molecular identification of the fungal species collected from nature was determined. Later, the dried waste biomass of the fungal species and MCM-41 were combined in different ratios to produce a bio-based adsorbent (bioadsorbent). The effects of pH, the initial dye concentration, bioadsorbent composition, bioadsorbent amount, and the contact time on RR120 removal by the new bioadsorbent were determined and optimized using artificial neural network (ANN) modeling. According to the results of this study, the optimal conditions for dye biosorption were determined. The maximum RR120 removal was achieved using the 1.67 g/L of bioadsorbent having fungi/MCM-41 (1:1) at pH 4 with an initial dye concentration of 20 mg/L after 60 min. Maximally 94.75% of RR120 has been removed. The results of FT-IR, XRD, and SEM-EDX analyses proved the adsorption of dye on the bioadsorbent surface. According to the results, the bio-based adsorbent developed in this study suits contaminated water with textile dye as an effective, biocompatible, environmentally friendly, and inexpensive adsorbent.

## Credit Author Statement

Veli ŞİMŞEK: Conceptualization, Methodology, Formal analysis, Investigation (MCM41 Synthesis and bioadsorbent characterization studies), Writing – original draft, Writing – review & editing; Rahmiye Zerrin YARBAY ŞAHİN: Conceptualization, Methodology, Formal analysis, Investigation (Bioadsorbent preparation and dye removal studies), Writing – original draft, Writing – review & editing, Vedat MARTTİN: Formal analysis, Software, Writing – original draft; Ülküye Dudu GÜL: Supervision, Conceptualization, Methodology, Visualization, Investigation (Fungi source, cultivation of fungi and molecular identification studies), Writing – original draft, Writing – review & editing.

## 1. Introduction

The advancement of science and technology is critical for a healthy living environment, future generations, and a sustainable environment. Scientists are investigating various methods for developing new environmental catalysts and catalytic processes due to the global emphasis on environmentally friendly chemicals, manufacturing processes, and technologies. Mobile researchers discovered silica-derived and metal-containing M41S materials, which piqued scientists' interest due to their mesopores, homogeneous pore size distribution, and high surface areas, which can be used as catalyst supports, adsorption and separation (Şimşek, 2021). It is used in various industries, including bio-materials (Cao et al., 2016; Quargli et al., 2015) and adsorbents (Quargli et al., 2015).

* Corresponding author.
*E-mail addresses:* ulkuyedudu.gul@bilecik.edu.tr, ulkuyedudugul@gmail.com (Ü.D. Gül).

https://doi.org/10.1016/j.jclepro.2023.138448
Received 19 May 2022; Received in revised form 7 August 2023; Accepted 12 August 2023
Available online 15 August 2023

The textile industry is the leading industry branch in Turkey, covering 20% of the total industry (Yarbay Şahin, 2022). Reactive azo dyes are widely used in dyeing processes in the textile industry due to their simple dying procedures and good stability during washing. Charges of this kind of wastewater into receiving waters can be hazardous to exposed organisms because of their reactivity, toxicity, and stability (Çelekli et al., 2012). More than 10,000 dyestuffs which cause the generation of approximately 280,000 tons of dyed wastewater per year, are used in the textile industry (Mass and Chaudhari, 2005). The dyes in wastewater generated from textile production harm the receiving environment's water and aquatic life. Dye accumulation in the receiving environment in organisms in water results in the formation of toxic and carcinogenic products (Kocaer and Alkan, 2002).

The most important effects of synthetic dyes on human health include carcinogenesis, mutagenesis, allergies, dermatitis, and skin irritation (Hamzezadeh et al., 2022). Some techniques such as ion exchange, membrane separation, electrochemical treatment (Barakat, 2011), adsorption (Varghese et al., 2019), catabolic enzymes (Guo et al., 2020), chemical precipitation (Kumar et al., 2021), reverse osmosis and electrolysis (Agaraw and Bogale, 2021), flotation (Aragaw et al., 2021), photocatalytic (Sharma et al., 2021) coagulation and flocculation (Sivaranjanee and Kumar, 2021) are used to reduce the harmful effects of dyes in wastewater. Its widespread use in wastewater treatment is sometimes limited due to its higher cost. Nonconventional sorbents of various types have been studied for their ability to remove contaminants from wastewater. Efforts are being made to develop low-cost materials to use as new adsorbents, such as nanomaterials (Mudhoo et al., 2021), graphene-based composites, and bio-adsorbents. Bioadsorbents like fungi, bacteria, and yeast are the most recent materials used to remove dyes and other pollutants in various industries (Kumar et al., 2021). Biomass-based adsorbents are gaining popularity and are being extensively researched due to their eco-friendly, low-cost, and good surface properties. It has been observed that the bioadsorbent production method used in this study is more economical than other methods in terms of both adsorbent source and method. It was determined that the newly suggested bioadsorbent has better results than other adsorbents regarding dye removal efficiency (Şimşek et al., 2019; Sharma et al., 2021).

Previously, different catalysts have been employed to remove the RR120 azo dye. Yu et al. (2019) synthesized silver nanoparticles from *Eriobotrya japonica* (Thunb.) leaf extract and utilized them to remove RR120. Using *Eriobotrya japonica* (Thunb.) leaf extract at pH 7, 20 °C, and a 1:10 ratio of silver nitrate applied to the leaf extract, the results indicated a bio-green strategy for generating AgNPs with a compact size and stable degrading activity of reactive dyes over 92% in 30 min (Yu et al., 2019). Rostamizadeh et al. (2018) decolored RR120 using a reusable Fe-ZSM-5 nanocatalyst. Its findings revealed that the best operating conditions for RR120 elimination (98%) were 1% Fe impregnation, 0.1 g nanocatalyst loading, and pH 3.0 (Rostamizadeh et al., 2018). Abidi et al. (2015) investigated the combined effects of dyes (RR120, Reactive Orange 84, and Reactive Blue 160), salts, and auxiliary chemicals used in the dyeing process on dye-containing effluent adsorption onto natural clay. The investigations demonstrated that the presence of all additives in the effluent increases dye adsorption (Abidi et al., 2015). Tehrani-Bagha et al. (2016) investigated magnetic copper ferrite nanoparticles for catalytic wet peroxide oxidation of the RR120 dye. They discovered that the best conditions for RR120 (50 mg/L) decolorization and COD removal were pH 3, 75 °C, 0.02 g/L catalyst dose, and 10 mM $H_2O_2$ (hydrogen peroxide), which was comparable to the Fenton process. With the use of $H_2O_2$ agents, it was completely removed (Tehrani-Bagha et al., 2016).

Reactive dyestuffs react with the textile fiber to form a covalent bond. They are used in these fiber classes because the reactive groups in their structures can react with cellulose, wool, silk, and polyamide. The reactive group is attached to the molecule's-colored part. The common feature of all reactive dyestuffs is that they all contain a reactive and a molecular solubility group and the colored group, carrying chromophores (Şimşek et al., 2019; David and Lewis, 2014). A thorough literature search reveals that many studies have been conducted on discovering novel adsorbents to remove textile dyes. Low-cost adsorbents with high adsorption capacity are important for a sustainable economy and ecology. After the discovery of support materials such as MCM-41, the use of heterogeneous catalysts has expanded day by day. In this study, MCM-41, produced using economical methods, was used as an effective bioadsorbent additive. To produce an environmentally friendly, biocompatible, and inexpensive bioadsorbent with potential usage in wastewater treatment containing textile dyes, the macro-fungus growing on its own in nature and being easily obtained has been selected to produce the efficient bioadsorbent. This study recommended a non-toxic, economical, and novel bioadsorbent developed using *Suillus collinitus* and MCM-41 for the first time in the literature. The bioadsorbent developed in the study can be used effectively in the treatment of RR120 shown in the results, as well as other dyestuffs with a reactive azo dye chemical structure and other pollutants that may have similar chemical properties.

This study investigated the removal of Reactive Red 120 dyestuff from the aqueous medium by modifying with the *S. collinitus* wastes and MCM-41 (a novel bioadsorbent) material at different durations, pH, loading rates, and concentrations. The results obtained were modeled using an artificial neural network (ANN) better to understand the adsorption process and optimal conditions of experiments. Owing to their ability to reliably and successfully define both linear and nonlinear relationships between multiple input-output factors, ANN methods are commonly used in a variety of research fields (Bishop, 1995) such as dye removal (Wang et al., 2022), chemical (Gholami et al., 2021). Data-driven modeling is an innovative approach to understanding the adsorption processes of various pollutants.

In this paper, RR120 dyestuff was removed with a novel bioabsorbent material. The results of removing RR120 were evaluated using two error functions ($R^2$ and RMSE). It was determined that this study, which was carried out using waste bio-absorbent and a low MCM-41 amount, was more economical in terms of cost. Although RR120 is close to each other in terms of removal, MM11 is calculated to be more economical. MM 11 (new bioadsorbent) is 5.26 times cheaper than commercial MCM-41. Comparisons of the calculation are given in detail in section 3.5. The RR120 dye removal values of fungi and MCM-41 were obtained as 29% and 88%. The RR120 dye removal value of MM11 (fungi/MCM-41; 1:1) was calculated as 94.75%.

## 2. Materials and methods

The bioadsorbent was consistent with two components: MCM-41 and *Suillus collinitus*. MCM-41 was obtained using the hydrothermal method. Since ancient times, *Suillus collinitus* has been classified using various morphological methods successfully to classify fungi. Developments in molecular biology and genetics in recent years have led to the emergence of new techniques in the field of fungal systematics (Naranjo-Ortiz and Gabaldón, 2020). The current study uses the 5.8 S rRNA gene to identify the fungus. Nuclear and mitochondrial rDNA regions such as 18 S rDNA, 28 S rDNA, and ITS and protein-coding genes such as RPB1, RPB2, and EF-1α are widely used in phylogenetic studies on fungi. Since protein synthesis is an ancient and common feature in all organisms, rRNAs are superior molecules for distinguishing the evolutionary relationship between organisms (Raven, 2013). FT-IR (Fourier Transform Infrared spectroscopy) is proposed as a fast, non-destructive, reliable, sensitive, and cost-effective technique that can be used to characterize the chemical composition (or functional groups) of various microorganisms (Fadlelmoula et al., 2022). FT-IR spectra are highly specific for each microbial species, and the FT-IR spectroscopy method can be successfully applied for fungal identification (Oberle et al., 2015; Bekiaris et al., 2020).

### 2.1. Chemicals

All chemicals used in fungi's molecular identification experiments were purchased from Sigma. The reagents used in MCM-41 preparation can be found in the reference (Şimşek et al., 2019). Reactive Red120 (Sigma) was chosen for the adsorption experiments at room temperature. It was produced by Sigma with CAS Number 61951-82-4 and used as received without further purification. The molecular weight of RR120 is 1469.98 g/mol. The chemical structure of this reactive azo dye can be found elsewhere (Şimşek et al., 2019).

### 2.2. Cultivation of fungi and molecular identification

The macro-fungus used in this study were collected from Sivas (Center) (Coordinate: 39° 75′ 05″ N and 37° 01′ 50″ E) in October 2020 and brought to the laboratory in sterile ziplock bags. The fungal samples were washed with distilled water twice. After a morphological examination of the fungal sporocarp (Fig. 1), the fungus was cultured in the laboratory.

The cultured fungal cells were used for 5.8 S rRNA gene amplification to identify the fungal species. The rDNA (5.8 S) region was amplified with primers given in Table (1). The amplification step in the PCR assays was performed by an initial denaturation at 95 °C for 30 s. Then 30 cycles were performed as denaturation, annealing, and elongation steps at 95, 50, 72, and 72 °C for 30 s, 30 s, 1 min, and 7 min. The used sequencing and phylogenetic analysis in the current study were previously defined by Biswas et al. (2001); Fell et al. (2000).

The waste fungal particles formed after the molecular identification step were dried at 60 °C in the oven for 24 h and pulverized as a cheap bio-based adsorbent additive in the adsorbent preparation step.

### 2.3. Neural network modeling

In Fig. 2, A1-AN *represents* data inputs in the IL, bias indicates the threshold value, and w1-wN represents the input data weights. The training function processes the incoming input data according to the training function and transmits it to the activation function as an x output. According to the activation function, y output is obtained in the output layer (OL). The results are then measured according to the input data, and the obtained results of the ANN are compared. Modeling is done according to the optimum neural network (NN).

This study created a multi-layer ANN, as seen in Fig. 3 (Hagan et al., 1996). To train the ANN, the min-max normalization process of the laboratory data was calculated as shown in Eq. (1) (Hagan et al., 1996), and the data was distributed in the 0–1 range. In the equation, $x_{new}$ represents the newly calculated value between 0 and 1, $x_{old}$ denotes the calculated value which is desired in the dataset. min $(x_{old})$ and max $(x_{old})$ denote the minimum and maximum values in the dataset.

$$x_{new} = \frac{x_{old} - \min\,(x_{old})}{\max\,(x_{old}) - \min\,(x_{old})} \tag{1}$$

To find the error rate of the ANN, the estimated value and the measured value from the laboratory were calculated according to the least squares method (RMSE). In Eq. (2)) (Hagan et al., 1996), in calculating the RMSE value, $n$ represents the number of data in the dataset, $q\,pred$ represents the value estimated by ANN, and $q\,exp$ denotes the value measured in the laboratory. The RMSE value is expected to be low.

$$RMSE = \frac{1}{n}\sqrt{\sum_{k=1}^{n}(q\,pred - q\,exp)^2} \tag{2}$$

In Eq. (3) (Hagan et al., 1996), in the calculation of the $R^2$ (regression) value, $n$ represents the number of data in the dataset, $q\,pred$ denotes the value estimated by ANN, $q\,exp$ represents the value measured in the laboratory, and $q\,avg\_exp$ represents the arithmetic mean of the values.

$$R^2 = 1 - \frac{\sum_{k=1}^{n}(q\,pred - q\,exp)^2}{\sum_{k=1}^{n}(q\,pred - q\,avg\_exp)^2} \tag{3}$$

Fig. 3 depicts constructing a three-layer feed-forward back-propagation model concerned with sorption parameters. FFNet (Feed-forward networks) comprises a series of interconnected layers from the IL (input layer) to the last layer, with no feedback connections. If it has enough neurons in its HL, an FFNet with a single HL (hidden layer) can be applied to any finite input-output mapping problem (Hagan et al., 1996). The incorrect use of neurons in the HL can prevent the ANN model from correctly generating predictions (Yargic et al., 2021). ANN models with various combinations of training and activation functions were created in this study. The number of neurons used in the ANN model is (5-6-1), (5-7-1), (5-8-1), (5-9-1), (5-10-1), (5–25) −1), (5-50-1) and (5-50-1). (5-100-1). In this case, the order is IL, HL, and OL. The laboratory environment's pH, duration (min), concentration (mg/L), MCM-41 ratio, and catalyst amount (g) were used as input data in the IL. In the ANN training, 70% of the training data, 15% of the validation data, and 15% of the test data were randomly separated and used in the data set. Levenberg-Marquardt (trainlm) was used to achieve the ANN training function. To train different numbers of neurons in the HL, logsig, purelin, and tansig were used. In the OL, the Purelin transfer function is used. Each ANN model was run with 1000 epochs and tested at least 20 times before the best data was chosen. Matlab software determined the numbers of neurons in the HL neurons, transfer functions, and training algorithms among the created ANNs (vR 2016b).

**Fig. 1.** Sporocarp of *Suillus collinitus* used in the current study.

### 2.4. Preparation of bio-based adsorbent

Silica-based MCM-41 was synthesized using the hydrothermal method in this study using the recipe published by Simşek (Şimşek et al., 2019). After obtaining MCM-41, MCM-41 and fungi (together named as *bio-based adsorbent*) were mixed in various ratios (Fungi/MCM-41 b y weight; 1:10, 1:4, 1:2, 1:3, and 1:1). Fungi and MCM-41 modifications were carried out in 50 mL of distilled water for 24 h at a mixing speed of 300 rpm and room temperature. The samples were dried at 65 °C for 24 h and kept in a desiccator. The samples were named MM 12, MM 11, MM 0.5, MM 0.25, and MM 0.10. Fungi, spent fungi, MCM-41 catalyst, and spent MCM-41 catalyst were assigned M, SM, MCM-41, and SMCM-41. The spent bio-based adsorbent samples were denoted as SMM11,

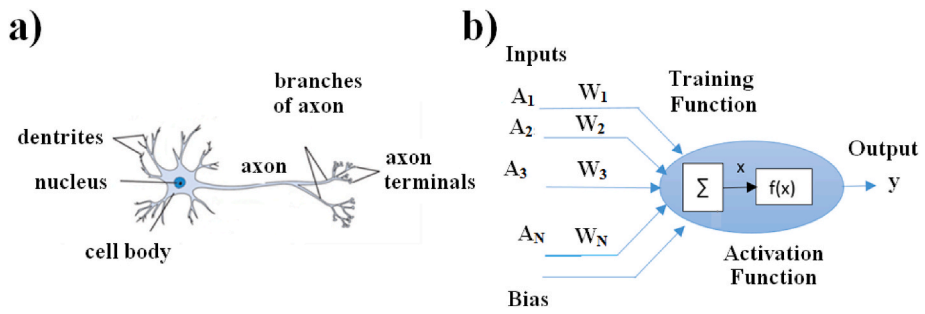


**Fig. 2.** (A) Biological nerve cell, (b) Artificial NN.

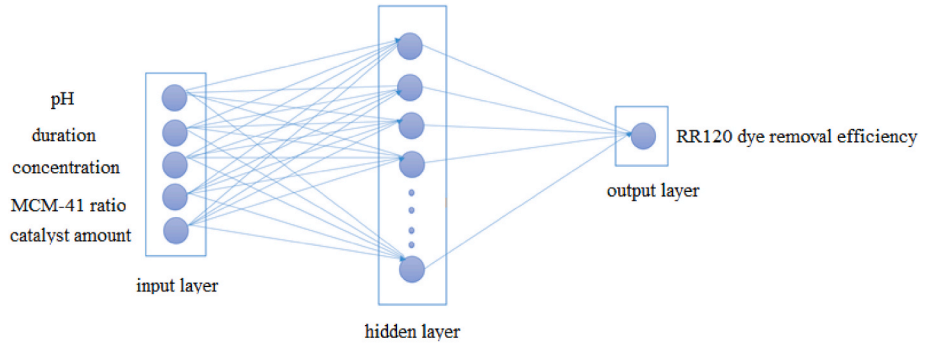


**Fig. 3.** Multi-layer ANN model.

SMM12, SMM0.5, SMM0.25, and SMM0.10 represents fungi to MCM-41 ratio by weight 1:1, 1:2, 1:0.5, 1:0.25, and 1:0.10.

### 2.5. Optimization of biosorption experiments

The removal of RR120 dyestuff with bio-based adsorbent began with pH optimization. For this purpose, 20 mL solutions of RR120 dyestuff have been adjusted to pH: 1, 2, 4, 6, and 8 in the present of Fungi/MCM-41: 1/1 bio-based adsorbent. The dye and bio-based adsorbent were mixed on a magnetic stirrer (400 rpm) in 35 mL beakers during adsorption experiments. The adsorbent and dye solutions were then separated by centrifugation at 7000 rpm for 5 min, and the remaining unadsorbed dye concentration was determined using a UV spectrophotometer at 522 nm (Şimşek et al., 2019). As a result of pH optimization studies, the best result was obtained with pH:4. All parameters, including effects of dye concentration, type of biosorbent, catalyst amount, and contact time, were investigated at pH 4.

The removal of RR120 dyestuff with bio-based adsorbent began with pH optimization. For this purpose, 20 mL solutions of RR120 dyestuff have been adjusted to pH: 1, 2, 4, 6, and 8 in the present of 1/1 bio-based adsorbent (Fungi/MCM-41). It was mixed for 1 h on a magnetic stirrer (400 rpm) in 35 mL beakers with 0.05 gr of bio-based adsorbent. The adsorbent and dye solutions were then separated by centrifugation at 7000 rpm for 5 min, and the remaining unadsorbed dye concentrations were determined using a UV spectrophotometer at 522 nm. As a result of pH optimization studies, the best result was obtained with pH:4. All analyses (effects of dye concentration, biosorbent type, catalyst amount, and contact time) were investigated at pH:4.

### 2.6. Adsorbent characterization assays

This study investigated the physical properties of MCM-41, Fungi, and Bio-based adsorbent materials before removing RR120 dyestuff from aqueous solutions. SEM (Scanning electron microscope), XRD (X-ray diffraction), and FT-IR characterization methods were carried out in detail. SEM micrographs of the fresh and spent bioadsorbents were attained in Zeiss Supra VP 40. Phase identification of the M, MM11, and used bioadsorbents (SMM11, SMCM-41) was carried by Panalytical Empyrean diffractometer at 40 kV under Ni-filtered CuKα radiation ($\lambda = 0.15418$ nm) 40 mA current, 45 kV tension, and 0.0131303 step range. Before the FT-IR analyses, the waste fungal samples were dried and powdered to a particle size of less than 2 mm (Bekiaris et al., 2020). SEM was conducted to analyze the surface morphology of bio-based adsorbent, fungi, and MCM-41 before and after RR120 dye adsorption. FT-IR spectrometer (Agilent Cary 630 Spectrometer) was employed to identify the functional groups of bio-based adsorbent, fungi, and MCM-41 before and after RR120 adsorption.

## 3. Results and discussion

### 3.1. Molecular identification

The base sequence results obtained in molecular identification studies were displayed by the Refgen company (Ankara, Turkey). The obtained sequences were compared with NCBI reference sequences to determine the species of isolate. For this purpose, the Basic Local Alignment Search Tool (BLAST) program was used. The DNA sequence obtained from the comparison showed 100% similarity with the samples identified as *S. collinitus* collected from the Lille region of France in 2014 under *Pinus wallichiana*. *S. collinitus* samples collected within the scope of this study are stored. The sporocarp morphology of the fungus used in this study (Fig. 1) also overlaps with the morphological structure of the sporocarp of *Suillus collinitus* (Sarwar and Khalid, 2014). The *Suillus collinitus* fungus species, which was identified using morphologic and molecular analyzes, was cultured and kept in the culture collection (Prof. Dr. Ülküye Dudu GÜL) in Bilecik Şeyh Edebali University Engineering Laboratories. Since this species is cultivated, it can be used sustainably for the production of bioadsorbent by being developed again in the processes where it is needed.

The FT-IR results of dried fungal samples were also investigated to support the identification results (Fig. 3 a). Bombalska et al. (2013) collected bands specific to certain functional groups of biological origin, seen in the infrared spectra of fungi, in three main regions: fatty acids (3050-2800 $cm^{-1}$), amide I and II (1700-1500 $cm^{-1}$), polysaccharides (1200 -900 $cm^{-1}$) (Bombalska et al., 2013) (Fig. 3 a).

### 3.2. Bio-based adsorbent characterization

#### 3.2.1. FT-IR

FT-IR analyses were carried out using the Agilent equipment. It was performed using ATR (Attenuated Total Reflectance) technique between 4000 and 400 $cm^{-1}$ wavelengths. FT-IR analysis results obtained are given in Fig. 4(a–d). Asymmetrical and symmetrical stretching vibrations (SVs) of the Si–O–Si were attributed to 1053 and 960 $cm^{-1}$. The band at approximately 672 $cm^{-1}$ demonstrated bending vibrations (BVs) of the Si–O–Si groups. On the other hand, the absorption band at 444 $cm^{-1}$ corresponds to the bending vibration of Si–O–Si (Yarbay Şahin, 2022; Lin et al., 2019; Benhamou et al., 2009; Zhao et al., 2014). Peaks of 1621cm−1 and 3403cm−1 indicated the –OH SVs of silanol groups and the BVs of adsorbed water (Fig. 4 (a, b)) (Shahbazi et al.,

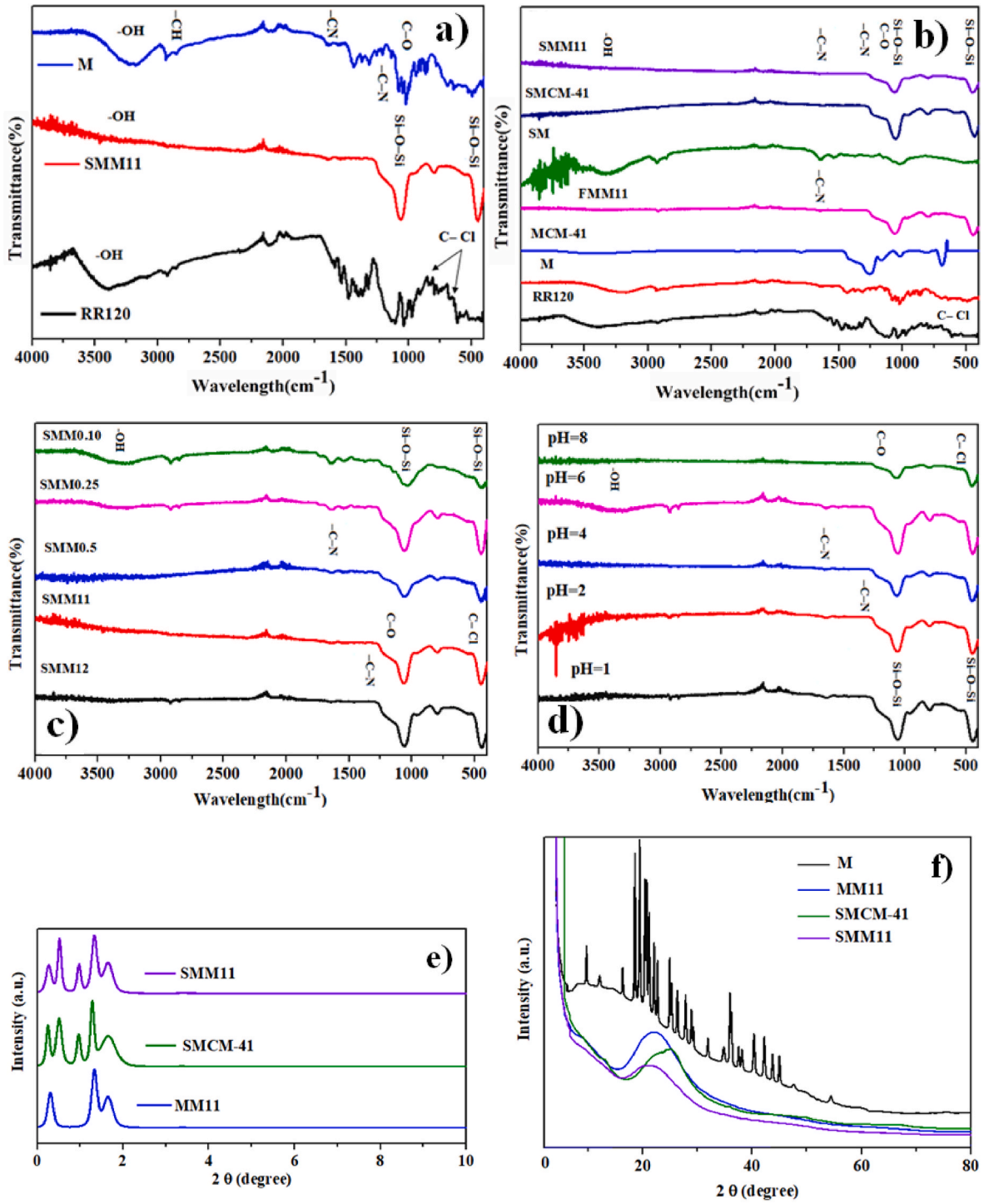


**Fig. 4.** A) FTIR analyses of samples ((SMM11; spent fungi/MCCM-41; W/W:1/1, M; fresh fungi) and RR120; reactive red 120), b) (SMM11; fungi/MCCM-41; W/W:1/1), (SMCM-41; spent MCM-41), (SM; spent fungi), (MCM-41; fresh), (M; fungi), (RR120; reactive red 120), c) FTIR analyses of samples (spent fungi/MCM-41; W/W; 1:2, 1:1, 1:0.5, 1:0.25 and 1:0.10), d) Different pH(SMM11), XRD diffraction diagrams of MM11, SMCM-41 and SMM11 (e), M, MM11, SMCM-41 and SMM11 (f) samples (M; fungi, MM11; fungi/MCM-41; 1:1, SMCM-41; spent MCM-41, SMM11; spent fungi/MCM-41; 1:1). (For interpretation of the references to color in this figure legend, the reader is referred to the Web version of this article.)

2011).

Fig. 4 (a, b) shows the FTIR spectra of fungus (M) powder before the sorption of RR 120. The dye unloaded M powder spectrum revealed distinct major peaks at 3322 (between 3250 and 3600 $cm^{-1}$), 2923, 1600, 1530, 1232, 1055, 1028, and 1011 $cm^{-1}$. Peaks at 3322 and 2923 $cm^{-1}$ could be attributed to –OH and $–NH_2$ groups and –CH SVs (Çelekli et al., 2012). 1627, 1218, and 1058 $cm^{-1}$ are also important M bands. They are represented by the vibrations of –CN stretching, C–N stretching, and C–O stretching (Çelekli et al., 2019). When Fig. 4 (a, b and d) are examined, the changes were observed after dye adsorption depending on the stretching of different functional groups. For instance, one of the significant changes after RR120 sorption was observed in the 1600 $cm^{-1}$ region of the spent fungus (SM-used in bioadsorbent production), which expresses the C–N stretching according to the literature. Presumably, this region on the surface of the fungus plays an important role in dye adsorption. Also, it is considered that the observed changes in the stretching of various functional groups on the fungus are associated with the interaction of dye molecules with active sites. Recent studies reported that electrostatic interactions are important in the chemical attraction of pollutants, such as metal ions, by the active sites of fungal adsorbents (Şenol et al., 2021). Vibration peaks of C–Cl were observed in the RR 120 spectra at 761–832 $cm^{-1}$ (Fig. 4 (a, b, c and d)) (Ge et al., 2017). The main peaks of MCM-41 were found to have no peaks after sorption with different pH and loading ratios (Fig. 4 (d)). These results were compatible with the SEM analysis (Fig. 5 (c)). As a result, it was determined that MCM-41 mostly preserved its hexagonal structure after removing RR120 (Şimşek, 2019). When FT-IR results are evaluated, it is observed that functional groups on the bioadsorbent play an important role in removing RR120.

### 3.2.2. XRD

XRD analyses were performed on M, MM11, SMCM-41, and SMM11 samples. M, MM11, SMCM-41, and SMM11 samples were analyzed in the range of 2θ:0° to 80 (Fig. 4 (e, f)). The hexagonal structure of MCM-41 was identified after the removal of RR120 dye and modified with fungi by determining diffraction patterns in the low-angle range between 2Θ = 0–10° and four peaks corresponding to (100), (110), (200) (Şimşek, 2019) and (210) reflections of ordered mesophase (Fig. 4 (e, f)), and this demonstrated that the MCM-41 retained its mesoporous structures. Sharp peaks of the fungus were not observed after modification with MCM-41 (Fig. 4 f). On the other hand, the amorphous structure of the silica structure of MCM-41 was observed at 2Θ = 24.93, 21.87, 25.35, and 21.10° in the wide-angle analyzes of the samples (Fig. 4 (f)) (Yarbay Şahin, 2022).

### 3.2.3. SEM-EDX

Before and after RR120 removal, SEM analyses of M, MCM-41, and samples prepared in different mass ratios were performed. The obtained results are given in Fig. 5. In Fig. 5 (a), the fungi spores are clear and still clear after using the fungi in dye removal, as shown in Fig. 5 (b). Besides, the fungus spore structures (Fig. 5 (a) were observed to look like water-absorbed rice grains. SEM images of the MCM-41 catalyst in Fig. 5 (c) were similar to the literature (Yarbay Şahin, 2022). SEM image of the MM 11 sample (Fig. 5 (d), in which MCM-41 was physically mixed with fungi in a 1:1 ratio by weight, shows spores attached to the catalyst particles. This situation is observed for the spent MM11 sample (Fig. 5 (e), but after using MM11 in dye removal, the dye molecules are also observed in the image (Fig. 5 (f)).

EDX and MAPPING analyses of SMM11 samples were performed to investigate structural changes before and after RR120 removal (to determine the changes in the CI, Na, S, and N elements of the RR120 dyestuff), and results are given in Figs. 6 and 7. In particular, the S, CI, and Na elements do not exist in the structure of MCM-41, as can be seen in Fig. 6. Significant changes in SMM11 EDX and MAPPING were observed after RR120 removal. While the amount of potassium, hydrogen, zinc, and copper was very high in the fungi sample (Fig. 6), the bioadsorbent material (Fig. 7) consisted mainly of silicium and oxygen from the mesoporous MCM-41 structure, besides zinc and nitrogen from the fungi structure. The images of samples at different pH and loading rates are given in supplementary data1 (Figs. 1 and 2).

## 3.3. Biosorption experiments

Herein, fungi: MCM-41 containing bio-based adsorbent type material prepared were used to remove the RR120 dye from water in terms of parameters like pH, the initial dye concentration, bioadsorbent composition, bioadsorbent amount, and the contact time. The results are shown in Fig. 8.

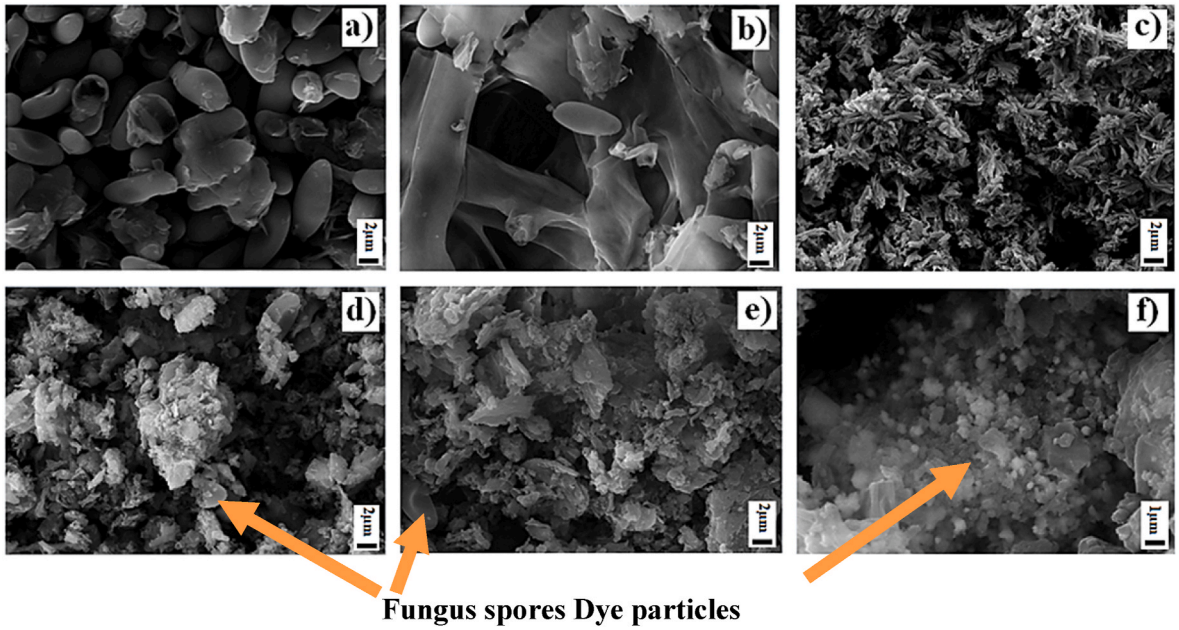


**Fig. 5.** SEM images of samples a) M; fungi, b) SM; Spent fungi, c) MCM-41, d) FMM11(Fresh fungi MCM-41), e) SMM11, 5kx (Spent fungi MCM-41) and f) SMM11, 10kx (Spent fungi MCM-41).

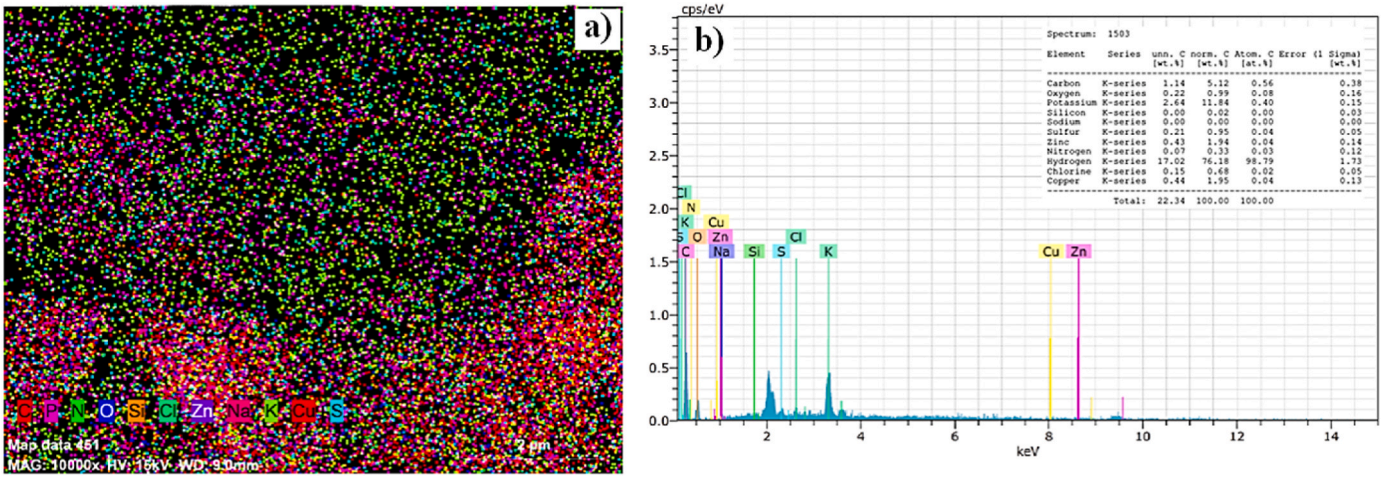


**Fig. 6.** MAPPING(a) and EDX (b) analysis of FM (Fresh fungi).

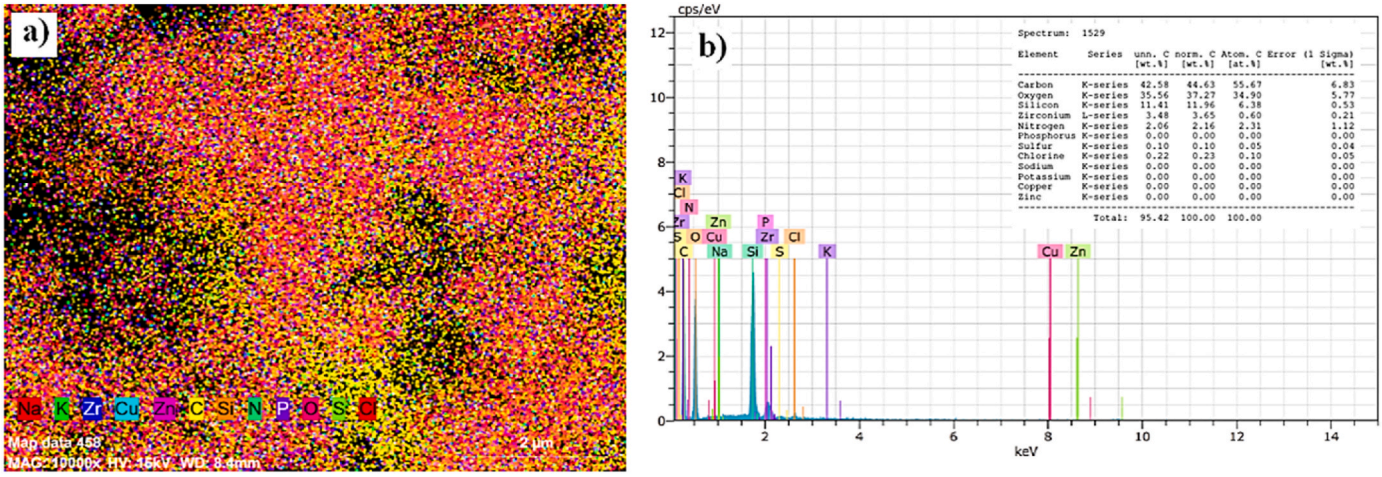


**Fig. 7.** MAPPING(a) and EDX (b) analysis of fresh MM11(Fungi/MCM-41; 1:1).

### 3.3.1. *The effect of pH*

The pH of the solution is an important parameter influencing the dye adsorption in view of its control of the adsorptive molecule's ionization degree (Jawad et al., 2020a, 2020b) and the adsorbent's surface charge (Sharma et al., 2018; Jawad et al., 2020a, 2020b). The effect of initial pH on the dye removal onto bio-based adsorbent, fungi, and MCM-41 was performed at different pH levels, including 1, 2, 4, 6, and 8 while fixing the other parameters like 0.05 g/35 mL adsorbent dosage, 20 mg/L dye concentration, and 60 min contact time. According to Fig. 8 (a), dye adsorption highly depends on the solution pH. The adsorption capacity of the dye was slightly increased from 11.23 to 12.11 mg/g when the pH increased from 1 to 4. The maximum adsorption efficiency was obtained at 4, and this pH was used for further experiments.

To the best of our knowledge, studies related to RR120 dye were carried out at different pHs like 2 (Ayachi et al., 2019; Anastopoulos et al., 2021), 3 (Jawad et al., 2020a, 2020b), and 4 (Khan et al., 2020) widely. Only a few studies were conducted at pH 1 (Çelekli et al., 2019). For instance, Khan et al. studied the decolorization of 20 mg/L RR120 dye at pH 4, 7, and 9 using the $Nb_2O_5NC$ photoanode. Their results showed that the degradation of RR120 was achieved as 100% of dye removal at pH 4 after 120 min Of treatment (Khan et al., 2020).

Fig. 8 (a) indicates negative adsorption on bio-based adsorbents, especially at pH 6 and 8. Other researchers also noticed this abnormal situation in the literature (Armağan and Turan, 2004). Armağan et al. explained that their adsorbent (zeolite) could not adsorb dye molecules due to their smaller pore size than the dye molecule. They observed that their adsorbent adsorbed water molecules instead of dye molecules resulting in an increment of the concentration measured, which is consistent with our results when pH was 6 or 8. Their comment about this situation was related to their adsorbent zeolite's silicate nature with $H^+$ and $OH^-$ ions which material was negatively charged in the pH region. As a result, they expected that any anionic dye groups would be repelled from the negatively charged zeolite surface, especially in the case of pH 7 or 8. When it is vital to conduct the adsorption in a basic environment, the adsorption capacity can be enhanced if the adsorbent is modified with a typical quaternary amine surfactant (HTAB) to hydrophobize the surface of zeolite and neutralize the negative charges (Armağan and Turan, 2004).

From the point of view of MCM-41, one of the important components of the bio-based adsorbent, the point of zero charges (PZC) and surface charge are important values to be taken into account. Şimşek et al. reported that the surface charge of the MCM-41 and SBA-15 were measured as −16.9 and −21.8 mV (Cardoso et al., 2012). Besides, the PZC of MCM-41 fired at 550 °C was measured as 4.87 in the literature (Monash and Pugazhenthi, 2010). They claimed that the favorable adsorption of dye on MCM-41 could only occur if the solution pH is higher than the pHpzc. At higher pH (>4), the pH of the solution is greater than the pHpzc of the MCM-41 (4.87), favoring the dye adsorption on MCM-41 (Yarbay Şahin, 2022). On the other hand, RR120 dye, known for its six sulphonates ($R–SO_3^-$) groups which have the pKa

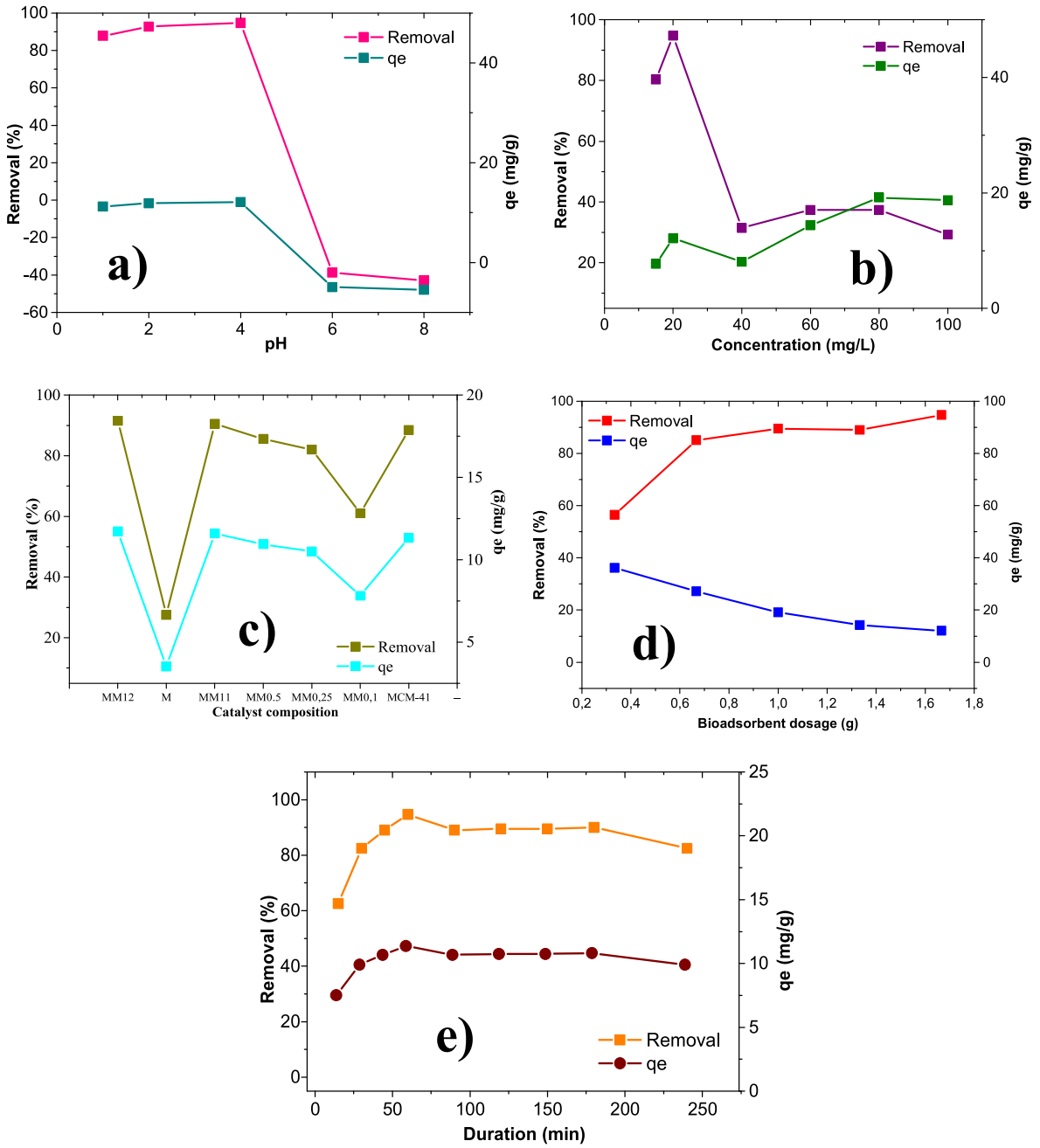


**Fig. 8.** Effect of a) pH, b) dye concentration, c) catalyst composition, d) catalyst dosage, and e) contact time on dye removal.

value of 2.1, can be readily dissociated in an aqueous solution, leaving the dye molecule with a net negative charge, as shown in the above (Munagapati et al., 2019; Khan et al., 2020):

$$RR120 - SO_3Na \rightarrow RR120 - SO_3^- + Na^+$$

$$S - OH \overset{H^+}{\rightarrow} S - OH_2^+ + RR120 - SO_3^- \rightarrow S - OH_2^+ > - - - < RR120 - SO_3^-$$

$$S - OH \overset{OH^-}{\rightarrow} S - O^- + RR120 - SO_3^- + H_2O \rightarrow S - O^- < - - - > RR120 - SO_3^-$$

Here S denotes the surface of the adsorbent.

In the literature, it is noticed that in the case of lower pH, the positively charged active sites of the adsorbent intrigue the negatively charged dye that upgrades the dye removal. For higher pH, the plenty of hydroxide ions challenges with dye and the ionic repulsions between the negatively charged surface and dye molecule outcomes lower dye uptake (Munagapati et al., 2019). The outer surface of the biosorbent does not expect to lay out exchangeable anions at higher pH values like 6 and 8, highlighting the lower pH as the suitable environment for the adsorption of a reactive dye using fungi-MCM-41 bio-based adsorbent. Experimental results align with previous studies (Munagapati et al., 2019; Khan et al., 2020).

### 3.3.2. *The effect of dye concentration*

It is critical from an application aspect to explore the initial concentration of dye on adsorption. Because the initial concentration plays an essential role in eliminating all mass transfer resistance of dye between the aqueous and solid phases, a certain solid mass can absorb only a limited amount of the dye (Subash et al., 2013). The initial dye concentration experiments were done by changing initial dye

concentrations in the range of 15–100 mg/L on 0.050 g of bio-adsorbent at pH 4 and for a contact time of 60 min. As shown in Fig. 8 (b), the removal was reduced when the initial RR120 concentration was increased. The maximum adsorption efficiency decreased from 94.75 to 31.5% when the dye concentration increased from 20 to 40 mg/L. This situation can be related to the turbidity effect in the case of a high dosage of bioadsorbent prohibiting the adsorption ability of the bio-adsorbent surface. According to Mansouri et al. (2021), increasing the initial dye concentration leads to catalyst surface filling. Most active sites may be covered with dye ions in case of high dye concentration (Mansouri et al., 2021). According to the study by Mahmoodi (2014), raising the initial dye concentration might result in interference from intermediates upon degradation of the parental dye molecules (Mahmoodi, 2014). The results follow previous results obtained by Boubakri et al. (2018).

#### 3.3.3. The effect of bioadsorbent type

The bioadsorbent type effect on the RR120 uptake was investigated using fungi, MCM-41, and various fungi: MCM-41 ratios by weight like 1:2, 1:1, 1:0.5, 1:0.25, and 1:0.1 at fixed volumes of 35 mL. Aimed at this effect, other parameters were kept constant at 296 K, contact time of 60 min, and pH at 4 for 20 mg/L RR120 concentration. The results in Fig. 8 (c) reflect that fungus had the lowest adsorption ability among the materials used. Adding fungi to MCM-41 displayed a synergistic effect as increasing the dye uptake in the case of adding the MCM-41 with the ratios of 1:2, 1:1, and 1:0.5. It was found that fungi: MCM-41 ratios of 1:1 and 1:2 showed similar removal uptake. Decreasing the MCM-41 amount in the bio-based adsorbent composition highlighted a significant decrease in the adsorption performance. The increment in the dye removal with the MCM-41 addition compared to only fungi used adsorption was related to the development in the available adsorbent surface area, as the number of adsorption sites raised as well (Jawad et al., 2019). The fungi: MCM-41 ratio of 1:1 was selected for subsequent work.

#### 3.3.4. The effect of bioadsorbent dosage

Bioadsorbent dosage is an essential factor that can significantly influence dye removal. To explore this effect, the experiments were conducted at different amounts of bio-adsorbent (0.33–1.67) with 20 mg/L dye concentration and 0.05 g adsorbent dosage for 60 min. The results in Fig. 8 (d) showed that the dye uptake increased with the increase in the amount. This situation can be clarified in light of the availability of active sites on the bioadsorbent surface. The total active surface area is reported to enhance by raising the bioadsorbent amount in the literature (Subash et al., 2013). As a result, 1.67 g/L was chosen as the optimal bioadsorbent dosage in this work.

#### 3.3.5. The effect of contact time

The contact time information provides insight into the more profound implication of the mechanism enabling the uptake of pollutants (Boubakri et al., 2018). It should be considered that the contact time is a fact that determines the optimum duration at which the equilibrium is obtained, especially at a laboratory scale (Abidi et al., 2019). Fig. 7 shows the contact time experiment results ranging from 15 to 240 min on 0.050 g of bio-based adsorbent at pH 4 for an initial dye concentration of 20 mg/L using 35 mL of dye. According to the results, the dye was rapidly taken out by the bioadsorbent in the first 60 min (Fig. 8 (e)). Later, the RR120 uptake declined until the equilibrium was observed after 120 min. Naghmouchi and Nahdi (2015) published similar results for the adsorption of RR120 using Tunisian raw clay (Naghmouchi and Nahdi, 2015). According to their findings, the adsorption phenomenon followed a linear path characterized by a quick rate at the initial step as long as there were sufficient unused adsorbent sites and a more significant concentration gradient between the LP and the solid-liquid interface. As time passed, the entrance to the remaining vacant surface sites was confined, the repulsive forces between the dye molecules on the solid and bulk phases were dispelled, and the result was a slower rate of adsorption known as the "plateau" effect (Boubakri et al., 2018). This explanation is valid for our contact time results as well. Also, similar tendencies for different types of dyes were observed in the literature (Hamzezadeh et al., 2022).

### 3.4. Application of neural network approach

In this research, combinations of training algorithms and transfer functions (tansig, logsig, and purelin for the HL and purelin transfer function for the OL) were used in this study to determine the ANN model with the highest forecast accuracy for every data set. Each model was tested with different neurons in their HL. ANN models were developed to forecast dye removal efficiency (percentage) accurately. As is well known, ANNs behave like a "black box" (McCulloch and Pitts, 1943); the error generates an output from the created models that varies from repetition to repetition. As a result, the measurements were repeated 20 times, and the best of the obtained error coefficients were presented as the outcome. ANN modeling was first performed using all removal results of M, MM11, and MCM41 given in Fig. 9. The results given in Table 2 show that the lm_tansig function obtained better results with a 5-8-1 network structure (0.994). Considering the 5-9-1 network structure, the lm_logsig function (Train's $R = 0.993$, $R^2 = 0.750$, and RMSE = 0.161) can be selected as the optimum ANN model. The low regression ($R^2 = 0.750$) value can be related to the very low removal capacity of RR120 using only fungi material (29%).

Table 3 shows the results obtained when there is without M during ANN training. According to the ANN training performance in Table 3 with the value of 0.998, the lm_tansig function obtains better results with the 5-100-1 network structure. Considering the $R^2$ and RMSE values, the 5-10-1 network structure with the lm_tansig function (Train's $R = 0.998$, $R^2 = 0.997$, and RMSE = 0.016) can be selected as the optimum ANN model.

Fig. 9(a–d) shows the Matlab software (program) regression curves for training the 5-10-1 network structure. By using ANN training, performance (Fig. 9 (a)), validation (Fig. 9 (b)), the performance of randomly (Fig. 9 (c)) selected test data, and regression values of all the data in the data set (Fig. 9 (d)) were obtained as 0.998, 0.999, 0.986 and 0.998.

According to the trained ANN data of the experiment results, the ANN model obtained with pH, duration (min), concentration (mg/L), MCM-41 ratio, and catalyst amount (g) is active on the IL is 5-9-1 l m_logsig. The best ANN model was obtained when the M factor is not active in the modeling is 5–10-1 l m_tansig. It has been determined that better results are obtained in ANN performances when M is not considered. As a result, it has been observed that the success of data-driven approaches depends on the consistency of real experimental results. In other words, it was determined that the ANN results of the adsorbent modified with fungi and MCM-41 were compatible with the selected experimental conditions. It has been observed that the selected experimental conditions are important to understand better the mechanism of the adsorption conditions in dye removal. These findings can be explained by the results of experiments in Fig. 8(a–e) and ANN in Fig. 9 (a–d).

### 3.5. Price comparison for commercial MCM-41 and MM11

One of the important points of this study is to obtain a novel cheap adsorbent. In this context, a cost comparison of the modified adsorbent with the commercial MCM-41 material was conducted. Calculations were made by considering all parameters (water, electricity, gas, and chemical) used to synthesize MCM-41. The price comparison for 5 g of the substance is given in Supplementary 2 Table 1.

## 4. Conclusion

In this research, the removal of RR120 dyestuff from the aqueous

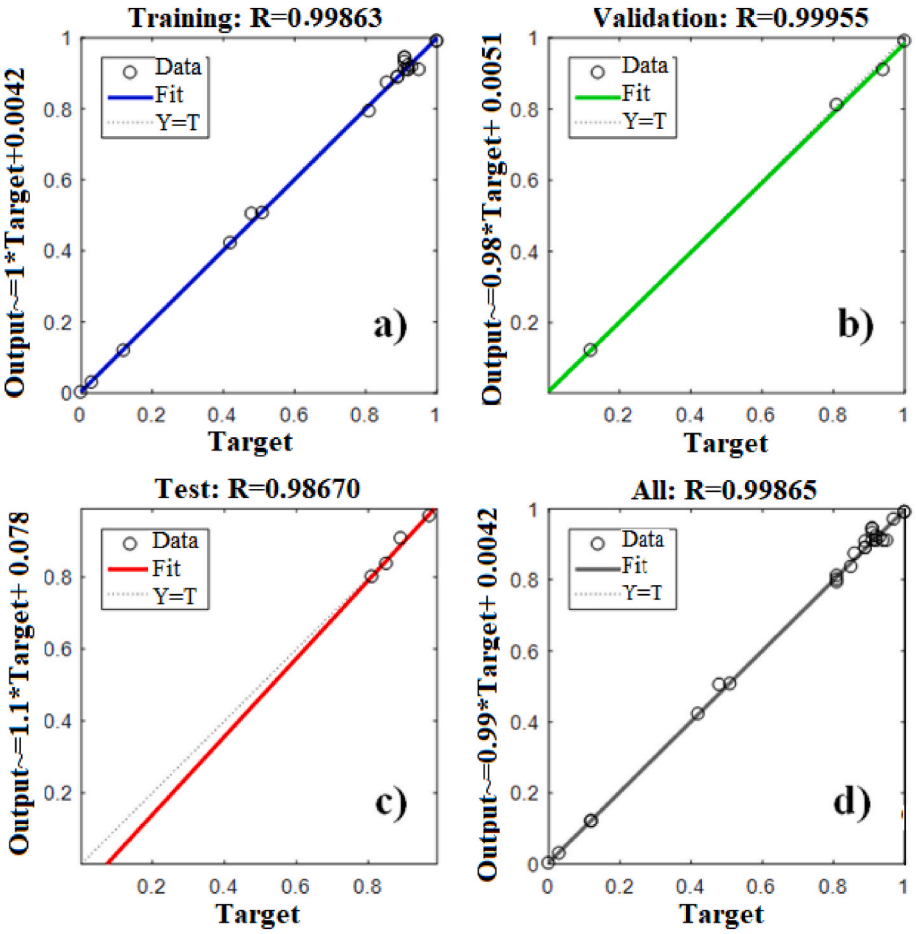


**Fig. 9.** The regression curves for the 5-10-1 ANN model.

**Table 1**
Primers used in PCR.

| | Primer | Reference |
|---|---|---|
| Forward | ITS1 50 -TCC GTA GGT GAA CCT GCG G-30 | Ferrer et al. (2001) |
| Reverse | ITS4 50 -TCC TCC GCT TTT GAT ATG C-30 | Ferrer et al. (2001) |

medium was investigated by modifying it with *Suillus collinitus* wastes and MCM-41 support material at different rates at pH, different durations, loading rates, and concentrations. The obtained results were modeled using an ANN to better understand the experiments' adsorption optimal conditions. The fungal sample's FT-IR results were examined to support the molecular and morphological identification results. Second, the MCM-41 was obtained using the hydrothermal synthesis method. MCM-41 and fungi were mixed in various ratios (Fungi/MCM-41 b y weight; 1:10, 1:4, 1:2, 1:3, and 1:1). In various ratios, bio-based MM (fungi/MCM-41) adsorbents were obtained by mass.

According to the results of this study, the optimal conditions were determined as fungi/MCM-41 = 1:1 with the adsorbent as pH 4, dye concentration 20 mg/L, adsorbent dosage 1.67 g/L, and contact time 60 min. Under these conditions, a maximum of 94.75% dye removal was achieved. Adsorption experiment conditions and the correlation between fungus and MCM-41 were investigated further, and the ANN model was used to predict RR120 under various influential factors.

This study provides helpful information about the factors influencing RR120 adsorption and a simple method for quantitatively evaluating and forecasting adsorption behavior with fewer parameters and high sensitivity. The removal efficiency of the adsorbent used in RR120 removal was 99% compatible with the results obtained with the ANN

**Table 2**
Results of ANN models to predict the adsorbent efficiency of RR120 dye (M, MCM-41, and MM11).

| Network training function | Activation function for hidden layer | Network structure | R | Training R | $R^2$ | RMSE |
|---|---|---|---|---|---|---|
| trainlm | lm_logsig | 5-6-1 | 0.842 | 0.983 | **0.686** | **0.181** |
| | lm_pureline | | 0.738 | 0.865 | **0.541** | **0.219** |
| | lm_tansig | | 0.845 | 0.985 | **0.694** | **0.178** |
| | lm_logsig | 5-7-1 | 0.830 | 0.999 | **0.662** | **0.188** |
| | lm_pureline | | 0.743 | 0.841 | **0.535** | **0.220** |
| | lm_tansig | | 0.822 | 0.958 | **0.662** | **0.187** |
| | lm_logsig | 5-8-1 | 0.829 | 0.899 | **0.687** | **0.180** |
| | lm_pureline | | 0.741 | 0.847 | **0.549** | **0.217** |
| | lm_tansig | | 0.804 | 0.999 | **0.609** | **0.202** |
| | lm_logsig | 5-9-1 | 0.866 | 0.993 | **0.750** | **0.161** |
| | lm_pureline | | 0.727 | 0.845 | **0.526** | **0.222** |
| | lm_tansig | | 0.831 | 0.961 | **0.688** | **0.180** |
| | lm_logsig | 5-10-1 | 0.836 | 0.988 | **0.692** | **0.179** |
| | lm_pureline | | 0.740 | 0.843 | **0.537** | **0.220** |
| | lm_tansig | | 0.808 | 0.964 | **0.641** | **0.193** |
| | lm_logsig | 5-25-1 | 0.816 | 0.998 | **0.628** | **0.197** |
| | lm_pureline | | 0.723 | 0.795 | **0.521** | **0.223** |
| | lm_tansig | | 0.853 | 0.843 | **0.722** | **0.170** |
| | lm_logsig | 5-50-1 | 0.830 | 0.931 | **0.680** | **0.183** |
| | lm_pureline | | 0.739 | 0.874 | **0.528** | **0.222** |
| | lm_tansig | | 0.812 | 0.977 | **0.603** | **0.203** |
| | lm_logsig | 5-100-1 | 0.822 | 0.969 | **0.672** | **0.185** |
| | lm_pureline | | 0.732 | 0.870 | **0.527** | **0.222** |
| | lm_tansig | | 0.831 | 0.880 | **0.678** | **0.183** |

**Table 3**
Results of ANN models to predict the adsorbent efficiency of RR120 dye (MCM-41 and MM11).

| Network training function | Activation function for hidden layer | Network structure | R | Training R | $R^2$ | RMSE |
|---|---|---|---|---|---|---|
| trainlm | lm_logsig | 5-6-1 | 0.981 | 0.976 | **0.963** | **0.059** |
| | lm_pureline | | 0.835 | 0.910 | **0.694** | **0.169** |
| | lm_tansig | | 0.967 | 0.998 | **0.934** | **0.078** |
| | lm_logsig | 5-7-1 | 0.995 | 0.996 | **0.991** | **0.029** |
| | lm_pureline | | 0.823 | 0.860 | **0.677** | **0.174** |
| | lm_tansig | | 0.795 | 0.765 | **0.606** | **0.192** |
| | lm_logsig | 5-8-1 | 0.991 | 0.999 | **0.982** | **0.040** |
| | lm_pureline | | 0.835 | 0.864 | **0.694** | **0.169** |
| | lm_tansig | | 0.998 | 0.999 | **0.997** | **0.016** |
| | lm_logsig | 5-9-1 | 0.995 | 0.995 | **0.988** | **0.032** |
| | lm_pureline | | 0.828 | 0.929 | **0.679** | **0.174** |
| | lm_tansig | | 0.984 | 0.999 | **0.968** | **0.054** |
| | lm_logsig | 5-10-1 | 0.992 | 0.990 | **0.991** | **0.028** |
| | lm_pureline | | 0.832 | 0.847 | **0.689** | **0.171** |
| | lm_tansig | | 0.998 | 0.998 | **0.997** | **0.016** |
| | lm_logsig | 5-25-1 | 0.930 | 0.925 | **0.857** | **0.116** |
| | lm_pureline | | 0.834 | 0.924 | **0.694** | **0.169** |
| | lm_tansig | | 0.950 | 0.943 | **0.898** | **0.097** |
| | lm_logsig | 5-50-1 | 0.967 | 0.965 | **0.918** | **0.087** |
| | lm_pureline | | 0.836 | 0.881 | **0.693** | **0.170** |
| | lm_tansig | | 0.997 | 0.999 | **0.994** | **0.023** |
| | lm_logsig | 5-100-1 | 0.998 | 0.996 | **0.996** | **0.019** |
| | lm_pureline | | 0.838 | 0.903 | **0.700** | **0.168** |
| | lm_tansig | | 0.637 | 0.999 | **−0.803** | **0.412** |

model. The ANN modeling analysis in this study showed that this modeling could be used to optimize adsorption studies to remove dyes and similar pollutants from wastewater. The ANN approach can be used to determine parameters for removing pollutants found in industrial wastewater. On the other hand, this paper highlights that the novel bioabsorbent, including waste fungi and MCM-41, was more economical in terms of cost. Previously, Gül (2013) showed that the micro-fungus (*Rhizopus arrhizus*) had minimum removal performance of Reactive Red dye among Reactive Blue and Reactive Black and removed 73.81% of Reactive Red dye. Ibrahim et al. (2017) reported that the macro-fungus (Pleurotus sp.) and micro-fungus (Aspergillus sp.) removed 29% and 63% of RR120. Şimşek et al. (2019) showed that the MCM-41 removed 94.73% of RR120. When these data in the literature are examined, it is seen that micro-fungus have the least removal of red dyes compared with other dyes having different properties. Micro-fungus has better dye removal performance than macro-fungus.

In this study, *Suillus collinitus,* a macro-fungus used for bioadsorbent production, is an edible fungal species that grows spontaneously in nature and has high antioxidant properties (Selem et al., 2021). No study has been found in the literature on the dye removal capacity of this species, according to our present knowledge. In this study, a macro-fungus that grows naturally was identified, and the usability of the waste fungus material obtained at the end of the preparation for identification studies as a stand-alone biosorbent and an inexpensive bioadsorbent additive was tested. The dye removal performance of MCM-41, which is produced at low-cost methods as shown in Section 3.5, as both adsorbent and bioadsorbent additive was determined. According to the results of this study, a macro-fungus *S. collinitus* (waste material) and MCM-41 removed 29% and 88% RR120 dye. The newly produced bioadsorbent (produced from a macro-fungus *S. collinitus* waste and MCM-41, with a 1:1 rate ratio) reached 94.75% RR120 removal potential. Since the ratio of MCM-41 used in producing newly developed bioadsorbent has been reduced by half, the cost has also decreased. As a result, in this study, a bioadsorbent with low cost and high dye removal performance was produced. Due to its abundance, the fungi in nature, *Suillus collinitus*, and MCM-41 together as a new bioadsorbent material can be considered a good, economically, and environmentally friendly absorbent. The results of this study contain preliminary information showing the successful usability of the developed bioadsorbent in textile industry wastewater. In the continuation of this study, it is recommended to carry out studies for scale-up and to focus on using bioadsorbent primarily at the lab-scale level and then in the bioreactor systems. Also, the data obtained from this study is a source for further studies on developing new bioadsorbents containing different biological sources or different MCM-41 derivatives obtained from alternative materials such as silica.

## Funding

This research received no specific grant from public, commercial, or not-for-profit funding agencies.

## Declaration of competing interest

The authors declare that they have no known competing financial interests or personal relationships that could have appeared to influence the work reported in this paper.

## Data availability

No data was used for the research described in the article.

## Acknowledgments

The author thanks Dr. Nevin Atalay Gengeç and Assoc. Prof. Dr. Erhan Gengeç for their support during the centrifuge operation step.

## Appendix A. Supplementary data

Supplementary data to this article can be found online at https://doi.org/10.1016/j.jclepro.2023.138448.

## Nomenclature (List of abbreviations)

| | |
|---|---|
| ANN | Artificial neural network |
| ATR | Attenuated total reflectance |
| BVs | Bending vibrations |
| EDX | Energy dispersive X-ray |
| FFNet | Feed-forward networks |
| FM | Fresh fungis |
| FMM11 | Fresh fungi/MCM-41; 1:1 |
| FT-IR | Fourier transform infrared |
| HL | Hidden layer |
| IL | Input Layer |
| LPs | Liquid phases |
| MCM-41 | Mobil Composition of Matter |
| MM | Fungi/MCM-41 |
| MM11 | Fungi/MCM-41; 1:1 |
| OL | Output layer |
| PZC | Point of zero charge |
| rDNA | Recombinant deoxyribonucleic acid |
| rRNA | Ribozomal ribobucleic acid |
| RMSE | Least squares method |
| RR120 | Reactive Red 120 |
| $R^2$ | Regression squared |
| SEM | Scanning electron microscope |
| SMCM-41 | Spent MCM-41 |
| SMM11 | Spent Fungi/MCM-41; 1:1 |
| SVs | Stretching vibrations |
| UV | Ultraviolet |
| XRD | X-ray diffraction |

## References


Abidi, N., Errais, E., Duplay, J., Berez, A., Jrad, A., Schäfer, G., Ghazi, M., Semhi, K., Trabelsi-Ayadi, M., 2015. Treatment of dye-containing effluent by natural clay. J. Clean. Prod. 86, 432–440. https://doi.org/10.1016/j.jclepro.2014.08.043, 2015.

Abidi, N., Duplay, J., Jada, A., Errais, E., Ghazi, M., Semhi, K., Trabelsi-Ayadi, M., 2019. Removal of anionic dye from textile industries' effluents by using Tunisian clays as adsorbents. Zeta potential and streaming-induced potential measurements. Compt. Rendus Chem. 22 (2–3), 113–125.

Anastopoulos, I., Pashalidis, I., Kayan, B., Kalderis, D., 2021. Microplastics as carriers of hydrophilic pollutants in an aqueous environment. J. Mol. Liq., 118182

Aragaw, T.A., Bogale, F., M, 2021. Biomass-based adsorbents for removal of dyes from wastewater: a review. Front. Environ. Sci. 9, 764958 https://doi.org/10.3389/fenvs.2021.764958.

Armağan, B., Turan, M., 2004. Equilibrium studies on the adsorption of reactive azo dyes into zeolite. Desalination 170 (1), 33–39.

Ayachi, F., Lima, E.C., Sakly, A., Mejri, H., Lamine, A.B., 2019. Modeling of adsorption isotherms of reactive red RR-120 on spirulina platensis by statistical physics formalism involving interaction effect between adsorbate molecules. Prog. Biophys. Mol. Biol. 141, 47–59.

Barakat, M.A., 2011. New trends in removing heavy metals from industrial wastewater. Arab. J. Chem. 4 (4), 361–377.

Bekiaris, G., Tagkouli, D., Koutrotsios, G., Kalogeropoulos, N., Zervakis, G.I., 2020. Pleurotus mushrooms content in glucans and ergosterol assessed by ATR-FTIR spectroscopy and multivariate analysis. Foods 9 (4), 535. https://doi.org/10.3390/foods9040535.

Benhamou, A., Baudu, M., Derriche, Z., Basly, J.P., 2009. Aqueous heavy metals removal on amine-functionalized Si-MCM-41 and Si-MCM48. J. Hazard Mater. 171, 1001–1008.

Bishop, C.M., 1995. Neural Networks for Pattern Recognition. Oxford University Press, New York.

Biswas, S.K., Yokoyama, K., Nishimura, K., Miyaji, M., 2001. Molecular phylogenetics of the genus Rhodotorula and related basidiomycetous yeasts inferred from the mitochondrial cytochrome b gene. Int. J. Syst. Evol. Microbiol. 51, 1191–1199.

Bombalska, A., Kaliszewski, M., Kwaśny, M., Mularczyk-Oliwa, M., Kopczyński, K., Szpakowska, M., Włodarski, M., 2013. Rapid discrimination of several fungus species with FTIR spectroscopy and statistical analysis. Biuletyn Wojskowej Akademii Technicznej 62 (3), 71–80.

Boubakri, S., Djebbi, M.A., Bouaziz, Z., Namour, P., Jaffrezic-Renault, N., Amara, A.B.H., Kalfat, R., 2018. Removal of two anionic reactive textile dyes by adsorption into MgAl-layered double hydroxide in aqueous solutions. Environ. Sci. Pollut. Control Ser. 25 (24), 23817–23832.

Cao, Z., Du, P., Duan, A., et al., 2016. Synthesis of Mesoporous Materials SBA-16 with Different Morphologies and Their Application in Dibenzothiophene hydrodesulfurizationChemical Engineering Science, vol. 155, pp. 141–152.

Cardoso, N.F., Lima, E.C., Royer, B., Bach, M.V., Dotto, G.L., Pinto, L.A., Calvete, T., 2012. Comparison of Spirulina platensis microalgae and commercial activated carbon as adsorbents for the removal of Reactive Red 120 dye from aqueous effluents. J. Hazard Mater. 241, 146–153.

Çelekli, A., İlgün, G., Bozkurt, H., 2012. Sorption equilibrium, kinetic, thermodynamic, and desorption studies of Reactive Red 120 on Characontraria. Chem. Eng. J. 191, 228–235.

Çelekli, A., Al-Nuaimi, A.I., Bozkurt, H., 2019. Adsorption kinetic and isotherms of Reactive Red 120 on Moringa oleifera seed as an eco-friendly process. J. Mol. Struct. 1195, 168–178.

David, M., Lewis, D.M., 2014. Developments in the chemistry of reactive dyes and their application processes, Color. Technol. 130, 382–412. https://doi.org/10.1111/cote.12114.

Fadlelmoula, A., Pinho, D., Carvalho, V.H., Catarino, S.O., Minas, G., 2022. Fourier transform infrared (FTIR) spectroscopy to analyse human blood over the last 20 Years: a review towards lab-on-a-chip devices. Micromachines 13, 187. https://doi.org/10.3390/mi13020187.

Fell, J.W., Boekhout, T., Fonseca, A., Scorzetti, G., Statzell-Tallman, A., 2000. Biodiversity and systematics of basidiomycetous yeasts as determined by large-subunit rDNA D1/D2 domain sequence analysis. Int. J. Syst. Evol. Microbiol. 3, 1351–1371.

Ferrer, C., Colom, F., Frasés, S., Mulet, E., Abad, J.L., Alió, J.L., 2001. Detection and identification of fungal pathogens by PCR and by ITS2 and 5.8S ribosomal DNA typing in ocular infections. J. Clin. Microbiol. 39 (8), 2873–2879.

Ge, S., Xu, Y., Jia, L., 2017. Secondary organic aerosol formation from ethylene ozonolysis in the presence of sodium chloride. J. Aerosol Sci. 106, 120–131.

Gholami, A., Khoshdast, H., Hassanzadeh, A., 2021. Applying hybrid genetic and artificial bee colony algorithms to simulate a bio-treatment of synthetic dye-polluted wastewater using a rhamnolipid biosurfactant. J. Environ. Manag. 299, 113666 https://doi.org/10.1016/j.jenvman.2021.113666.

Gül, Ü.D., 2013. Treatment of dyeing wastewater including reactive dyes (reactive red RB, reactive black B, remazol blue) and methylene blue by fungal biomass. WaterSA 39 (5), 593–598.

Guo, G., Li, X., Tian, F., Liu, T., Yang, F., Ding, K., et al., 2020. Azo dye decolorization by a halotolerant consortium under microaerophilic conditions. Chemosphere 244, 125510–125537. https://doi.org/10.1016/j.chemosphere.2019.125510.

Hagan, M.T., Demuth, H.B., Beale, M.H., 1996. Neural Network Design. PWS Publishing, Boston, MA.

Hamzezadeh, A., Rashtbari, Y., Afshin, S., Morovati, M., Vosoughi, M., 2022. Application of low-cost material for adsorption of dye from aqueous solution. Int. J. Environ. Anal. Chem. 102 (1), 254–269.

Ibrahim, N.N., Talib, S.A., Ismail, H.N., Tay, C.C., 2017. Decolorization of reactive red-120 by using macrofungus and microfungus. J. Fund. Appl. Sci. 9 (6S), 954–964.

Jawad, A.H., Shazwani, N., Mubarak, A., Sabar, S., 2019. Adsorption and mechanism study for reactive red 120 dye removal by cross-linked chitosan-epichlorohydrin biobeads. Composites, Part B 75, 415–418.

Jawad, A.H., Mubarak, N.S.A., Abdulhameed, A.S., 2020a. Hybrid crosslinked chitosan-epichlorohydrin/TiO2 nanocomposite for reactive red 120 dye adsorption: kinetic, isotherm, thermodynamic, and mechanism study. J. Polym. Environ. 28 (2), 624–637.

Jawad, A.H., Mubarak, N.S.A., Abdulhameed, A.S., 2020b. Tunable Schiff's base-cross-linked chitosan composite for the removal of reactive red 120 dye: adsorption and mechanism study. Int. J. Biol. Macromol. 142, 732–741.

Khan, S.U., Perini, J.A.L., Hussain, S., Khan, H., Khan, S., Zanoni, M.V.B., 2020. Electrochemical preparation of $Nb_2O_5$ nanochannel photoelectrodes for enhanced photoelectrocatalytic performance in removal of RR120 dye. Chemosphere 257, 127164.

Kocaer, F.O., Alkan, U., 2002. Boyar madde içeren tekstil atıksularının arıtım alternatifleri. Uludağ Üniversitesi Mühendislik-MimarlıkFakültesi Dergisi 7 (1), 47–55.

Kumar, A., Singh, R., Kumar Upadhyay Sanjay Kumar, S., Charaya, M.U., Charaya, M.U., 2021. Biosorption: the removal of toxic dyes from industrial effluent using phytobiomass- a review. Plant Arch 21, 1320–1325. https://doi.org/10.51470/plantarchives, 2021.v21.s1.207.

Lin, Y., J Xu, J., Sudhakar, B.S., Gu, J., Hong, R., 2019. Preparation of spherical aminopropyl-functionalized MCM-41 and its application in removal of Pb(II) ion from aqueous solution. Nanotechnol. Rev. 8, 275–284.

Mahmoodi, N.M., 2014. Binary catalyst system dye degradation using photocatalysis. Fibers Polym. 15 (2), 273–280.

Mansouri, M., Sadeghian, S., Mansouri, G., Setareshenas, N., 2021. Enhanced photocatalytic performance of UiO-66-NH2/TiO2 composite for dye degradation. Environ. Sci. Pollut. Control Ser. 28 (20), 25552–25565.

Mass, R., Chaudhari, S., 2005. Adsorption and biological decolorization of azo dye Reactive Red-2 in semi continuous anaerobic reactors. Process Biochem. (Oxford, U. K.) 40, 699–705.

McCulloch, W.S., Pitts, W., 1943. A logical calculus of the ideas immanent in nervous activity. Bull. Math. Biol. 5 (4), 115–133.

Monash, P., Pugazhenthi, G., 2010. Investigation of equilibrium and kinetic parameters of methylene blue adsorption onto MCM-4. Kor. J. Chem. Eng. 27 (4), 1184.

Mudhoo, A., Mohan, D., Pittman, C.U., Sharma, G., Sillanpää, M., 2021. Adsorbents for real-scale water remediation: gaps and the road forward. J. Environ. Chem. Eng. 9 (I 4), 105380 https://doi.org/10.1016/j.jece.2021.105380.

Munagapati, V.S., Wen, J.C., Pan, C.L., Gutha, Y., Wen, J.H., 2019. Enhanced adsorption performance of Reactive Red 120 azo dye from aqueous solution using quaternary amine modified orange peel powder. J. Mol. Liq. 285, 375–385.

Naghmouchi, N., Nahdi, K., 2015. Adsorption of textile dyes on raw Tunisian clay: equilibrium, kinetics and thermodynamics. J Adv Chem 11 (6), 3685–3697.

Naranjo-Ortiz, M.A., Gabaldón, T., 2020. Fungal evolution: cellular, genomic and metabolic complexity. Biol. Rev. 95, 1198–1232. https://doi.org/10.1111/brv.12605.

Oberle, J., Dighton, J., Arbuckle-Keil, G., 2015. Comparison of methodologies for separation of fungal isolates using Fourier transform infrared (FTIR) spectroscopy and Fourier transform infrared-attenuated total reflectance (FTIR-ATR) microspectroscopy. Fungal Biol. 119 (11), 1100–1114. https://doi.org/10.1016/j.funbio.2015.08.007.

Quargli, R., Hamacha, R., Benharrats, Net al., 2015. β-diketone functionalized SBA-15 and SBA-16 or rapid liquid–solid extraction of copper. J. Porous Mater. 22, 511–520.

Raven, J., 2013. RNA function and phosphorus use by photosynthetic organisms. Front. Plant Sci. 4 (536), 1–13. https://doi.org/10.3389/fpls.2013.00536.

Rostamizadeh, M., Jafarizad, A., Gharibian, S., 2018. High efficient decolorization of Reactive Red 120 azo dye over reusable Fe-ZSM-5 nanocatalyst in electro-Fenton reaction. Sep. Purif. Technol. 192, 340–347. https://doi.org/10.1016/j.seppur.2017.10.041.

Sarwar, S., Khalid, A.N., 2014. Diversity and phylogeny of Suillus (suillaceae; boletales; basidiomycota) from coniferous forests of Pakistan. Int. J. Agric. Biol. 16, 489–497.

Selem, E., Alp, Y., Sensoy, S., Uzun, Y., Cavusoglu, S., Karatas, N., Ercisli, S., Yilmaz, N., Ekiert, H., Elansary, H.O., Szopa, A., 2021. Biochemical and morphological characteristics of some macrofungi grown naturally. J Fungi (Basel) 12 (10), 851, 7.

Şenol, Z.M., Gül, Ü.D., Gurbanov, R., Şimşek, S., 2021. Optimization the removal of lead ions by fungi: explanation of the mycosorption mechanism. J. Environ. Chem. Eng. 9, 104760.

Shahbazi, A., Younesi, H., Badiei, A., 2011. Functionalized SBA-15 mesoporous silica by melamine-based dendrimer amines for adsorptive characteristics of Pb(II), Cu(II) and Cd(II) heavy metal ions in batch and fixed bed column. Chem. Eng. J. (Lausanne) 168, 505–518.

Sharma, G., Kumar, A., Naushad, M., García-Peñas, A., Al-Muhtaseb, A.H., Ghfar, A.A., Sharma, V., Ahamad, T., Stadler, F.J., 2018. Fabrication and characterization of Gum Arabic-cl-poly(acrylamide) nanohydrogel for effective adsorption of crystal violet dye. Carbohydrate Polym. 202, 444–453. https://doi.org/10.1016/j.carbpol.2018.09.004.

Sharma, G., Kumar, A., Naushad, M., Thakur, B., Dai-Viet, N.V., Gao, B., Al-Kahtani, A. A., Stadler, F.J., 2021. Adsorptional-photocatalytic removal of fast sulphon black dye by using chitin-cl-poly(itaconic acid-co-acrylamide)/zirconium tungstate nanocomposite hydrogel. J. Hazard Mater. 416, 125714 https://doi.org/10.1016/j.jhazmat.2021.125714.

Şimşek, V., 2019. Investigation of catalytic sustainability of silica-based mesoporous acidic catalysts and ion exchange resins in methyl acetate synthesis and

characterizations of synthesized catalysts. Arabian J. Sci. Eng. 44, 5301–5310. https://doi.org/10.1007/s13369-018-3570-y.

Şimşek, V., 2021. Synthesis and characterization of Fe/SBA-15 heterogeneous catalysts for methyl acetate production. European Journal of Science and Technology 28, 21–28. https://doi.org/10.31590/ejosat.977591.

Şimşek, V., Pat, Z., Murtezaoğlu, K., 2019. Adsorption conditions investigation of reactive RED 120 dyes on the silica-based porous material. BSEU Journal of Science 6, 237–246. https://doi.org/10.35193/bseufbd.603274.

Sivaranjanee, R., Kumar, P., S, 2021. Treatment of textile wastewater using biochar produced from agricultural waste. Sustainable Technologies for Textile Wastewater Treatments 187–208. https://doi.org/10.1016/b978-0-323-85829-8.00004-3.

Subash, B., Krishnakumar, B., Swaminathan, M., Shanthi, M., 2013. Highly efficient, solar active, and reusable photocatalyst: Zr-loaded Ag–ZnO for reactive red 120 dye degradation with synergistic effect and dye-sensitized mechanism. Langmuir 29 (3), 939–949.

Tehrani-Bagha, A.R., Gharagozlou, M., Emami, F., 2016. Catalytic wet peroxide oxidation of a reactive dye by magnetic copper ferrite nanoparticles. J. Environ. Chem. Eng. 4 (2), 1530–1536. https://doi.org/10.1016/j.jece.2016.02.014.

Varghese, A.G., Paul, S.A., Latha, M.S., 2019. Remediation of heavy metals and dyes from wastewater using cellulose-based adsorbents. Environ. Chem. Lett. 17, 867–877. https://doi.org/10.1007/s10311-018-00843-z.

Wang, Q., Bian, J., Ruan, D., Zhang, C., 2022. Adsorption of benzene on soils under different influential factors: an experimental investigation, importance order and prediction using artificial neural network. J. Environ. Manag. 306, 114467 https://doi.org/10.1016/j.jenvman.2022.114467.

Yarbay Şahin, R.Z., 2022. A comparative study on dark adsorption of dyes using mesoporous MCM-41 catalyst. Res. Chem. Intermed. https://doi.org/10.1007/s11164-021-04631-3.

Yargic, A., Yargic, A.S., Ozbay, N., 2021. Utilization of factorial design methodology to optimize Pr Red Hegxl dye uptake and prediction of removal efficiency via artificial neural network: comparison of linear vs. nonlinear sorption isotherm and kinetic parameters. Biomass Conv. Bioref. https://doi.org/10.1007/s13399-020-01193-z.

Yu, C., Tang, J., Liu, X., Ren, X., Zhen, M., Wang, L., 2019. Green biosynthesis of silver nanoparticles using *Eriobotrya japonica* (thunb.) leaf extract for reductive catalysis. Materials 12, 189. https://doi.org/10.3390/ma12010189, 21.

Zhao, Y.G., Li, J.X., Zhang, S.W., Wang, X.K., 2014. Amidoxime-functionalized magnetic mesoporous silica for selective sorption of U(VI). RSC Adv. 4, 32710–32717.